IRAQI JOURNAL OF APPLIED PHYSICS
Vol. (14), No. (2), April-June 2018, pp. 11-18

Investigation of Bound and Free Surface Waves in Microwave and Acoustic Wind-Wave Tank Systems

Khalid S. Jameel [1]*
Genady Ibeshiyv [1]
Latia K. Parshieva [2]
Patrick J. Vodesko [2]

[1] *Applied Physics Laboratory University of Kharkov, Kharkov, UKRAINE*
[2] *Free Surface Wave Group, Institute of Astrophysics, Minsk, BELORUSSIA*

** Department of Physics, College of Science, Al-Anbar University, Al-Anbar, IRAQ*

Microwave and acoustic systems operated in the large wind-wave tank show that most small-scale waves produced at large angles to the wind are products of breaking events bound to longer waves in the tank. These longer waves propagate at the dominant wave phase speed for fetches near 7m but travel at speeds corresponding to the phase speed of a wave half as long as the dominant wave at fetches near 26m. The microwave and acoustic systems operated at both 8mm and 2cm wavelengths. Measurements were made at seven wind speeds, five incidence angles, seven azimuth angles, and two nominal fetches. Two peaks were found in either the microwave or acoustic Doppler spectrum when looking upwind or downwind, but never in both. The sum of these spectral densities, the total short wave spectral density, was similar to, but lower than, previous measurements. The nature of millimeter-length bound waves was found to be different at long fetch than at short fetches, a feature not observed in centimeter-length bound waves.

Keywords: Wind waves; Bound surface wave; Free surface wave; Acoustics
Received: 5 January 2018, **Revised**: 23 March 2018, **Accepted**: 30 March 2018

1. Introduction

For several years, investigations have shown that not all short surface waves on wind-roughened water surfaces are generated directly by the wind [1-7]. Rather, a significant fraction (up to 50%) of short surface waves with lengths in the centimeter and millimeter range are generated by longer waves through distortions, through the production of parasitic capillary waves, or through breaking [3,7]. Here we designate free waves to be short waves directly generated by the wind and bound waves to be those generated by longer waves. Bound waves are, in general, given a mean tilt by their parent waves and move at speeds near those of their parent waves, which is often much faster than their intrinsic phase speed.

While these past studies have determined the existence of bound and free waves on wind-roughened water surfaces, they have been unable to determine the angular dependence of bound and free waves separately. Furthermore, past studies have shown that bound waves travel at the speed of the dominant wave in tanks with fetches of 15 m or less while on the ocean they travel at speeds significantly smaller than that of the dominant wave [3,4,8]. At the short fetches, millimeter-length bound waves were shown to be parasitic capillary waves [4]. In this paper, we report experiments carried out in a large wind-wave tank. Coherent microwave and acoustic systems with wavelengths within 10% of each other were set up to view the same spot on the water surface at the same time at the same incidence angles and azimuth angles with respect to the wind. The measurements confirmed that both mean Doppler shifts (Doppler offsets) and cross sections could be explained on a bound wave/free wave model. The bound waves were found to travel at the dominant wave phase speed at fetches near 7m but at the phase speed of a wave half as long as the dominant wave at fetches near 26m. The millimeter-length bound waves responsible for backscattering 8 mm radiation were shown not to be parasitic capillary waves at fetches near 26m. Free wave spectral densities were found to drop rapidly to zero with increasing azimuth angle, becoming virtually undetectable at 55° to the wind. Bound waves were found to decrease much more slowly, or not at all, with azimuth angle. The sum of bound and free wave spectral densities deduced from fitting data to model were close to past measurements of total short wave spectral densities at various azimuth angles and wind speeds.

2. Experiment

The tank is 40 m long and 3 m wide. During our experiments, the water was 0.9 m deep and

the air channel was 1.5 m high. Wind was measured with a combination of Pitot tubes and hot film anemometers and reached a maximum speed of approximately 12.5 m/s at the center of the air channel. A capacitance wave gauge yielded omnidirectional variance spectra of surface wave height. Table (1) gives wind, wave, and fetch conditions during the runs reported here.

K_u (14GHz–2cm wavelength) and K_a (35GHz–8mm wavelength) band, continuous-wave, coherent microwave systems were operated from above the tank looking through a large window covered with polyethylene. The systems were both dual polarized so that VV and HH polarized returns could be obtained simultaneously. Henceforth, we will refer to these as the radars. Coherent, pulsed acoustic systems at 70 kHz (2 cm wavelength) and 190 kHz (8mm wavelength) were operated from below the water. Henceforth, we will call these systems the sonars. We arranged the radar and sonar so that they always viewed the same spot on the water surface at the same incidence and azimuth angles. This was ensured by floating a metal sphere on the water surface and maximizing the return from the sphere to both systems. A schematic side view of the experimental arrangement is presented in Fig. (1).

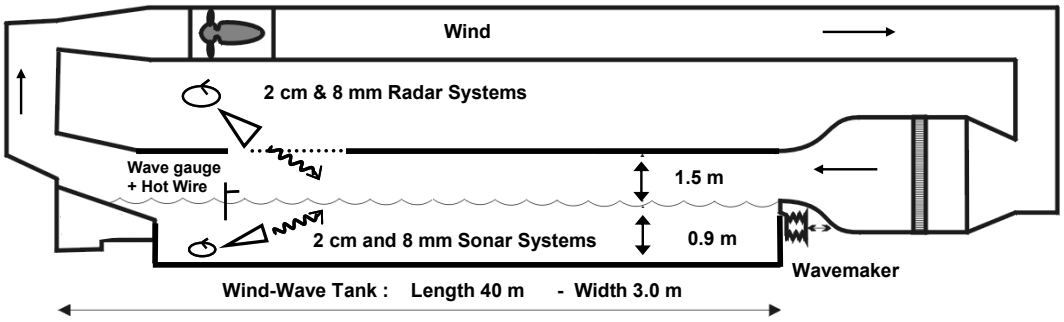

Fig. (1) Schematic side view of the experimental arrangement

Table (1) Wind, wave, and fetch parameters used during these experiments. U is wind speed, given at two heights; u* is friction velocity; Hs is significant wave height; □p is the dominant wavelength; and cp is the phase speed of the dominant wave as given by Plant and Wright (1980) for the measured u* and □p

Fetch	U@50cm	U@12 cm	u*	Hs	λp	cp
m	m/s	m/s	cm/s	cm	cm	cm/s
25.5	3.02	2.59	8.8	0.54	14.2	48.6
25.5	4.09	3.48	12.7	1.01	23.5	61.8
25.5	5.14	4.32	17.2	1.48	32.5	72.2
25.5	6.19	5.21	20.2	2.09	35.2	75.1
25.5	8.20	6.75	31.4	2.88	53.8	91.7
25.5	10.36	8.32	45.9	3.86	59.4	95.7
25.5	12.55	9.65	64.6	5.41	76.8	106.9
8.0	2.99	2.65	7.9	0.01	3.12	27.2
8.0	4.02	3.61	10.3	0.20	4.76	31.2
8.0	5.07	4.52	13.3	0.50	10.2	42.5
8.0	6.10	5.38	16.6	0.72	14.2	49.4
8.0	8.14	6.96	26.2	1.24	21.4	60.0
8.0	10.28	8.69	35.1	1.72	27.6	67.6
8.0	12.46	10.19	50.0	2.54	39.7	79.7

Figure (2) is a top view of the tank showing the locations of the centers of the various surface areas illuminated during the course of the experiment at various incidence and azimuth angles. The nominal fetch at the center of the circular pattern of illuminated spots was 27 m, but could be reduced to 8.2 m by covering the upwind water surface with plastic sheet.

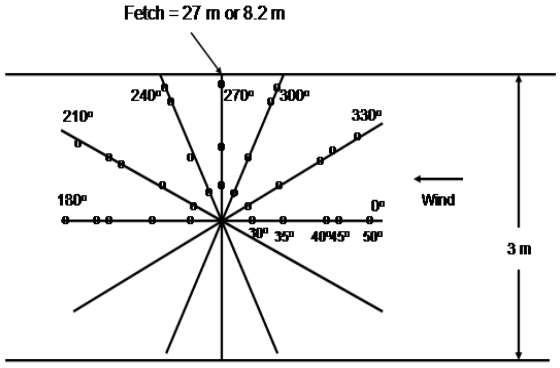

Fig. (2) Plan view of experimental arrangement showing the locations of the centers of the illuminated areas.

The fetch at the measured spot varied somewhat as the incidence and azimuth angles varied. The distance from the centerline to the outer illuminated spots (50^o incidence angle) was 1.7 m; to the inner spot (30^o incidence angle), it was 0.4 m. So, looking upwind, the

actual fetch of the illuminated spot varied from 25.3 m to 26.6 m (from 6.5 m to 7.8 m with the plastic sheet) depending upon the incidence angle. Most runs were made with the water uncovered although a few runs were made at the shorter fetch near the end of the experiments. In the calculations of the dominant wavelength, used below, the ±6% variations in fetch for different incidence and azimuth angles have been taken into account.

3. Results and Discussion

We made similar microwave and acoustic measurements at 2 cm and 8 mm in a short wind-wave tank. Comparison of the measurements made in the tank in 2011 with those previous measurements shows the consistency of the measurements and also indicates some differences in behavior between long and short fetches. Figure (6) compares measurements made using 2 cm wavelengths in the UW tank at a 5 m fetch and an incidence angle of 50^o with both radar and sonar looking upwind (red lines and symbols) with similar measurements made long (blue) and short (green) fetches. Measured cross sections (Fig. 3a) were nearly the same at all fetches, to within about 3 dB, at all wind speeds. In contrast, Doppler offsets, that is, the first moments of the Doppler spectra, (Fig. 3b) increase with fetch at most wind speeds. Furthermore, the increase in Doppler offset is greater from 5.0 to 6.5 m fetch than it is from 6.5 to 25.5 m.

Figure (4) shows cross sections and Doppler offsets measured at 8 mm wavelength and a 50^o incidence angle looking upwind in the UW tank and at long fetch in the tank; unfortunately, no short fetch data were collected at this wavelength. For this wavelength, the cross sections are different at the two fetches, the most dramatic difference being the peak in cross section at a friction velocity of about 0.18 m/s in the short fetch data. We have identified the backscatter at this wind speed, fetch, and wavelength to be a result of scattering from parasitic capillary waves [4]. A reasonable conclusion from Fig. (7) is that this is no longer the case at the longer fetch. Instead, the scatter appears to be due to other types of bound waves that exist at this fetch. We will return to this point below. Doppler offsets once again show an increase with fetch at all wind speeds.

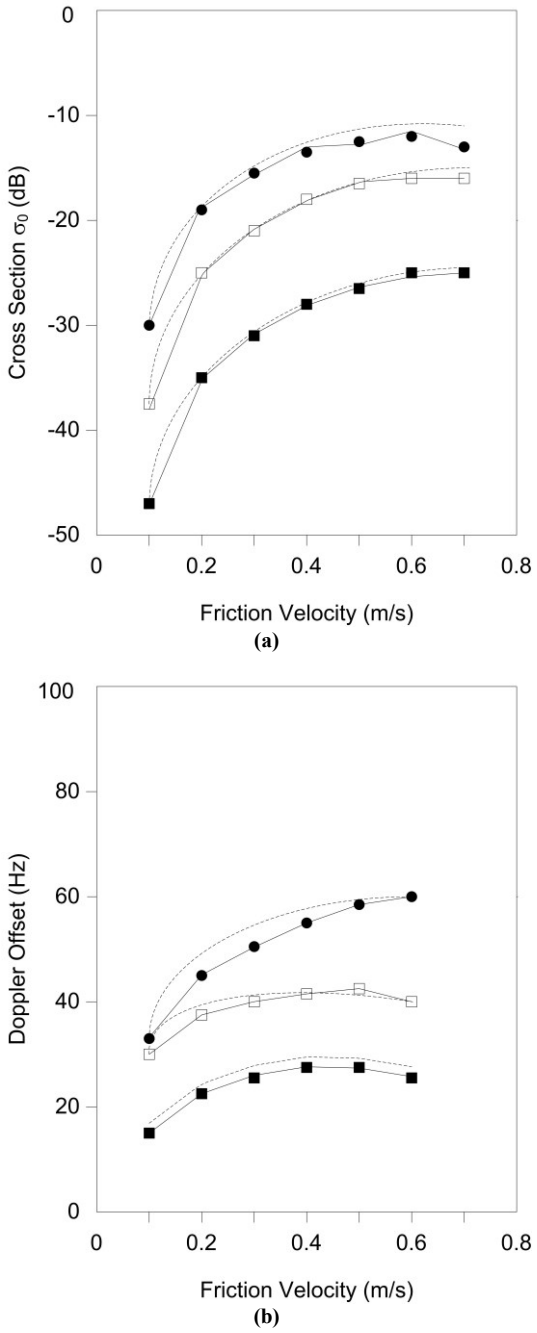

Fig. (3) (a) 2 cm cross sections versus friction velocity, (b) 2 cm Doppler offsets versus friction velocity. Data were taken at with 2 cm wavelength radiation and a 50^o incidence angle with both radar and sonar directed upwind. Symbols: + = sonar, x = radar HH, o = radar VV. Data at 5 m fetch (solid lines) were collected in 2005 in the UW wind-wave tank; those at 6.5 m (dotted lines) and 25.5 m fetches (dashed lines) were collected in 2011 in the large wind-wave tank

We have discussed our bound wave/free wave model of microwave backscatter from wind-roughened water surfaces many times in the past so we will be brief here. The model postulates that roughness is created by long, wind-generated waves on the leeward side of their crests as shown in Fig. (5). These are bound waves; they may be parasitic capillaries

or breaking wave products. Since they are localized on the long wave, they have a mean tilt in the downwind direction and are moving, if not exactly at the long wave phase speed, then very near it. Not shown in Fig. (8) are the free waves, which we picture as being generated directly by the wind, covering the surface outside of bound-wave regions, and traveling at their own intrinsic phase speed, as modified by the long-wave orbital velocity. We assume that the turbulence due to the bound waves in front of the long wave crest damps the free waves there. This is particularly valid at high winds where air flow separation at the crest of the dominant wave induces a reattachment of the air flow downwind far from the crest just behind the sheltered zone where the tangential stress drops. Therefore, the mean free wave slope is not zero but must be in the opposite direction to that of the bound waves in order that the overall surface slope be zero (or at least very small, since set-up occurs, especially in tanks).

Backscatter to microwave or acoustic systems is calculated according to this model by simply adding scattering due to bound waves to the standard Bragg/composite surface scattering theory [9-10]. The resulting normalized cross section (cross section divided by illuminated area) is then given by

$$\sigma_o = \sigma_c + \sigma_b$$

where the composite surface cross section σ_c and the bound wave cross section σ_b are given by

$$\sigma_c = \iint \sigma_B(\theta_o+\gamma, \alpha)\, P_f\, P(\gamma, \alpha \mid f)\, d\gamma d\alpha$$

$$\sigma_b = \iint \sigma_B(\theta_o+\gamma, \alpha)\, P_b P(\gamma, \alpha \mid b)\, d\gamma d\alpha$$

where θ_o is the nominal incidence angle, (γ, α) are the long wave slopes in and perpendicular to the plane of incidence, P_f is the probability of finding free waves, P_b is the probability of finding bound waves, and $P(\gamma,\alpha|x)$ is the probability distribution of a wave of type x, either free or bound, σ_B is the standard Bragg scattering cross section

$$\sigma_B = 16\, \pi\, k_o^4 |g(\theta_o+\gamma, \alpha)|^2\, F_x(2k_o \sin(\theta_o+\gamma), 0)$$

where g is a function of the dielectric constant and local incidence and tilt angles, k_o is the microwave number, and F_x is the wave height variance spectrum of either free or bound waves evaluated at $(2k_o \sin(\theta_o+\gamma), 0)$. More details, including the forms of g for VV and HH polarization may be found in [3]. Values of g for acoustic scattering are the same as those for HH electromagnetic Bragg scattering from a perfectly conducting surface.

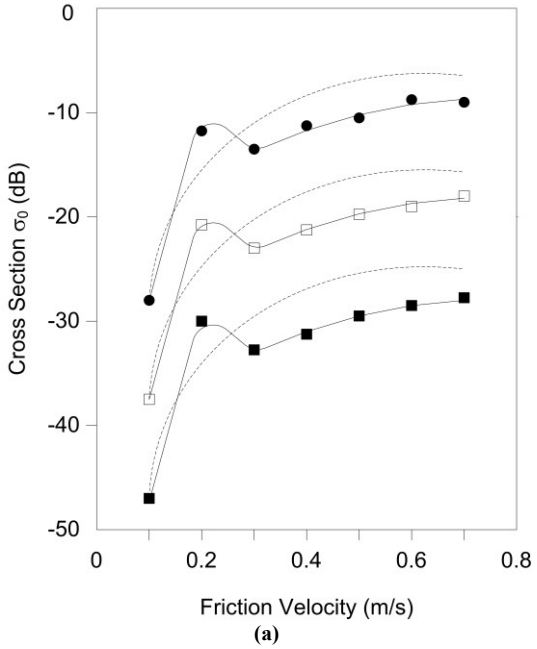

(a)

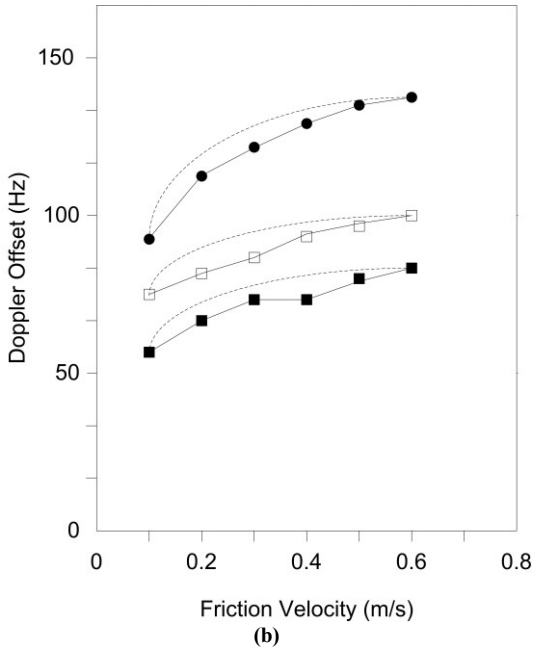

(b)

Fig. (4) Same as Fig. (6) but at 8 mm. No data were taken at short fetches in the tank at this wavelength

Doppler offsets may be calculated on this model as the weighted sum of Doppler shifts of scattering from free and bound waves, either of which may be calculated from

$$f_x = 2\, V \sin\theta_o / \lambda$$

where x is either f for free or b for bound waves. For free waves, V is the intrinsic phase speed of the Bragg wave, $\lambda_B=\lambda/(2\sin\theta_o)$

For bound waves, V is near the speed of propagation of the parent wave. Here λ is either the microwave or acoustic wavelength $(=2\pi/k_o)$. The total Doppler offset is therefore given by

$f_d = (\sigma_c f_f + \sigma_b f_b)/\sigma_o$.

Some observations about this model are in order. First, if a significant difference exists between the sonar cross section and the HH radar cross section, then tilting of the scatterers is indicated. This means that maxima of the conditional probabilities P are not at γ=0. If γ_b is the mean bound wave tilt, then the mean free wave tilt is

$\gamma_f = - P_b \gamma_b / P_f$

in order to give the overall surface zero slope. Second, the mean spectral density of either bound or free waves is given by

$<F_x> = F_x P_x$

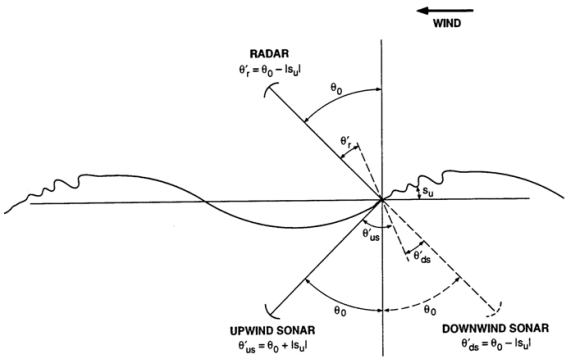

Fig. (5) The bound wave/free wave model showing the difference in local incidence angle when bound waves are viewed from above and below the water surface. Free waves are assumed to exist everywhere outside of the region of bound waves on the leeward face of the long wave

Third, in the model either changing the tilt or changing the mean spectral density will change the resulting cross section. Therefore, σ_b may be kept constant if $<F_x>$ is changed to compensate a change in tilt. Recall that the tilt of the bound waves must be set at a value that will yield the correct ratio of HH radar to sonar cross sections. Finally, the region where bound waves exist could be too rough to allow Bragg scattering to be a good approximation there. However, in the next section, data will be compared with the model based on Bragg scattering and the agreement is generally good.

Both the long wave slopes in and perpendicular to the plane of incidence affect the value of cross section computed. Since in these experiments, we looked at various azimuth angles with respect to the wind, and we assume that the bound wave tilt is all in the wind direction, the effective tilts in and perpendicular to the plane of incidence change as the azimuth angle changes. Also, we assume that the mean motion of the bound waves is in the direction of the wind so the component of the bound wave mean velocity in the direction of the azimuth angle is used in computing the bound wave Doppler offset.

4. Comparison of Data and Model

This bound wave/free wave scattering model was implemented in MATLAB and results were computed by adjusting free and bound wave spectral densities as a function of wavenumber to fit the data as well as possible. Values of the mean square slopes of free and bound waves are required for the calculation of the conditional probabilities P, which were assumed Gaussian; these and the values of P_b were obtained from the work of [3]. Mean tilts (slope angles) of the bound waves were adjusted from those given by [3] as required to fit the data, and free wave tilts were obtained from the equations of the previous section. P_f was obtained from P_b: $P_f = 1-P_b$.

At this azimuth angle, the fit of cross sections and Doppler offsets to the model could only be produced by setting bound wave spectral densities much larger than those of free waves. The two types of waves produced different effects because their mean tilts are constrained by the data at other azimuth angles. Thus the data indicate that short waves traveling at large angles to the wind are bound waves resulting from the crosswind irregularities of roughness regions associated with breaking. Here, we are referring to spilling, often microscale, breaking that does not have significant air entrainment [11].

The observation that the bound waves do not travel at the phase speed of the dominant wave for fetches near 26 m is intriguing because our previous work at 5, 10, and 12.5 m fetches has shown that they do travel with the dominant wave at those fetches [3-4]. On the other hand, the primary breaking waves on the ocean are definitely not the dominant waves [8,12]. To see whether the results in the tank were consistent with our previous measurements, we fit the model to the 2 cm data taken at 6.5 m fetch. The results are shown in Fig. (6). In this case, the measured Doppler offsets were best fit by assuming that the bound waves traveled at the dominant wave phase speed, in agreement with our previous measurements.

We collected data at seven different azimuth angles, as shown in Fig. (2). Those collected looking directly across the tank were not valid at any incidence angle due to backscatter from

the side. At the other azimuth angles, we were able to fit the data to the model as well as shown in the examples above. An exception was when the microwave and acoustic systems were pointed directly downwind. In this case the fit deteriorated somewhat, probably because of reflections of the microwave signals from the carriage on which the wind and wave measuring equipment was mounted. Several conclusions were supported by data at all incidence angles: bound and free waves have a mean tilt; bound waves travel at the dominant wave phase speed at short fetches but at the speed of a wave half as long at fetches near 26 m; and short waves traveling at large angles to the wind are not produced directly by the wind but by the breaking of longer waves.

The primary parameters adjusted to produce the fits between model and data shown in the previous section were the mean spectral densities of the free and bound waves. However, several other parameters were necessary in the model in addition to these spectral densities. Mean square slopes and the probabilities of finding free and bound waves used here were the same as those used by [3].

Figure (7) shows the mean tilt angles of the bound waves used to fit the data at the two different fetches in these experiments. Also shown in the figure are the mean bound wave tilt angles found in our previous experiments [3-4]. These slopes are negative to indicate that they are slopes on the leeward side of the long wave crest where the height of the long wave is decreasing in the direction of travel.

Using these slopes and the other parameters obtained in past experiments, we were able to derive mean spectral densities of free and bound waves individually at various azimuth angles and wind speeds. Their sum is the total short wave spectral density. We specified these spectral densities with a piecewise continuous function, each piece of which was given by $<F_x>=C_x k^{-n}$. Spectral densities of the curvature spectrum $B(k)=k^4<F_x>$ that produced the best fits to the data for waves traveling in the wind direction at various friction velocities are shown in Fig. (7). Total spectral densities measured by other investigators are also shown in the figure; our values appear to be somewhat lower than the other measurements.

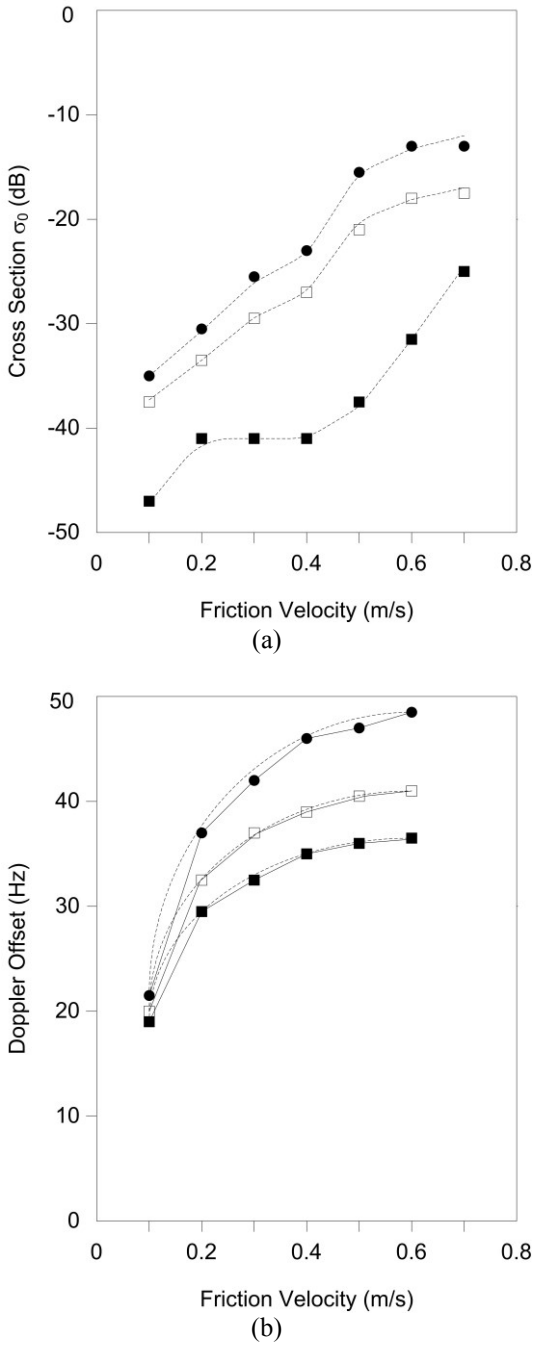

Fig. (6) Cross sections and Doppler offsets measured with 2 cm wavelength incident radiation at a 50° incidence angle looking upwind with a fetch of 6.5 m. The lines indicate the following: lower dashed = HH, bound waves move at their own phase speed; dotted = HH, bound waves move at the phase speed of the first harmonic of the dominant wave; dash-dotted = HH, solid = VV, upper dashed = sonar, all assuming bound waves move at the dominant wave phase speed

We have observed the properties of microwave and acoustic backscatter from a wind-roughened water surface in a large wind-wave tank using 2 cm and 8 mm wavelength radiation. We have shown that the data can be fit by a model that postulates that short surface waves are produced both directly by the wind (free waves) and indirectly by longer wind

waves (bound waves). Three properties of the received signals required that such a model be used rather than a model in which all waves are directly generated by the wind. One is that Doppler spectra obtained at moderate wind speeds with antennas and transducers looking in the same horizontal direction exhibit two peaks in either the microwave or acoustic spectrum, but never in both. The spectrum exhibiting two peaks switches from microwave to acoustic as the azimuth angle varies from upwind to downwind. The second property is that HH microwave cross sections differ in general from acoustic cross sections by much more than expected from a simple wind-wave model. This indicates that some of the scatterers have a mean tilt so that the local incidence angle at their location is different for radiation incident on the surface from above than from below. The third property is that first moments of the Doppler spectra, or Doppler offsets, show that some short waves on the surface move much faster than their expected phase speed.

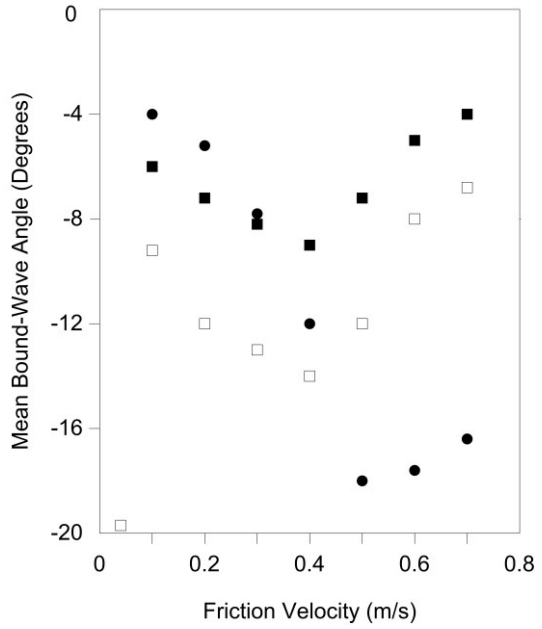

Fig. (7) Mean bound wave slopes measured in these experiments and in previous experiments. Symbols indicate the following fetches: □ = 6.5 to 7.8m, this experiment; ■ = 25.3 to 26.6 m, this experiment; ● = 5.0 m, Plant et al, 1999b; points = 14.3 m, Plant et al., 1999a. All values were derived from microwave and acoustic measurements except the points, which came from direct measurements using a laser slope gauge

The speed at which the bound waves move was found to be the phase speed of the dominant wave in the tank at fetches near 7m but to decrease to the phase speed of the first spatial harmonic of the dominant wave at fetches near 26m. This is in line with past observations that show that bound waves move at the dominant wave phase speed when the fetch is below about 15 m but that bound waves on the ocean move much more slowly than the dominant wave phase speed [3-4,8]. The work of [12] also showed that whitecaps on the ocean, which account for a small fraction of the bound waves, travel at speeds well below those of the dominant waves.

The dependence of the backscatter on azimuth angle with respect to the wind shows that spectral densities of free waves, i.e., those directly generated by the wind, fall rapidly for large azimuth angles. Bound waves, on the other hand, fall much more slowly with increasing azimuth angle, sometimes even appearing isotropic in our measurements. This conclusion came from both the cross section data and the Doppler offset data. Cross sections at large azimuth angles could not be fit with significant free wave spectral densities if the mean slopes of the bound and free waves were kept at the levels that fit data taken at smaller azimuth angles. Doppler offsets corresponded closely to the component of the bound wave velocity along the observed azimuthal direction and did not generally correspond to the expected phase speed of a free wave. These observations lead us to conclude that short surface waves on wind-roughened water surfaces that travel at large angles to the wind are manifestations of lateral roughness variations in the turbulent regions of breaking waves.

Finally, the present observations show that the bound, millimeter-length waves responsible for backscattering 8 mm incident radiation do not move at their intrinsic phase speed at long fetches. Previously in short fetch situations we found that these waves did move at their intrinsic phase speed, which was also the dominant wave phase speed [3]. This led us to identify the scatterers at these short fetches as parasitic capillary waves. Since at the longer fetches of this experiment, the speed of these bound waves is clearly different from their intrinsic phase speed, we conclude that they are primarily turbulence associated with spilling breaking rather than parasitic capillaries. This probably accounts for the much higher cross sections found for 8 mm wavelength radiation at low winds for short fetches than for long. It implies that spectral densities of parasitic capillary waves are larger than those associated

with breaking turbulence. The fact that the bound, centimeter-length surface waves that backscatter 2 cm wavelength radiation never move at their intrinsic phase speed shows that they are never parasitic capillary waves. This is because at these wavelengths it is not possible to match the speeds of gravity and capillary waves. This probably accounts for the similarity of cross sections for 2 cm wavelength radiation at low winds for long and short fetches.

Conclusions

The results of these experiments confirm our earlier findings that backscatter from wind-roughened water surfaces cannot be accurately explained without including effects of parasitic capillary waves and the regions of roughness associated with spilling or microscale breaking waves.

References

[1] Hara, T., Bock, E.J., and M. Donelan, *J. Geophys. Res.*, 102, 1061-1072, 1997.
[2] Fedorov, A.V., W.K. Melville, and A. Rozenberg, *Phys. Fluids*, 10, 1315-1323, 1998.
[3] Plant, W.J. et al., *J. Geophys. Res.*, 104(C2), 3243-3263, 1999a.
[4] Plant, W.J., P.H. Dahl, and W.C. Keller, *J. Geophys. Res.*, 104, 25,853-25,866, 1999b.
[5] Rozenberg, A.D., M.J. Ritter, and W.K. Melville, *IEEE Trans. Geosci. Rem. Sensing*, 37(2), 1052-1065, 1999.
[6] Plant, W.J., *J. Geophys. Res*., 108(C9), 3295, 2003a.
[7] Plant, W.J., *Waves in Random Media*, 13(4), 339-354, 2003b.
[8] Plant, W.J., *J. Geophys. Res*., 102(C9), 21131-21146, 1997.
[9] Bass, F.G. et al., *IEEE Trans. Antenna and Prop.*, AP-16(5), pp. 554-559, 1968.
[10] Wright J.W., *IEEE Trans. Ant. Prop.*, AP-16(2), 217-223, 1968.
[11] Jessup, A.T. et al., *Nature*, 385, 52-55, 1997.
[12] Melville, W.K., and P. Matusov, *Nature*, 417, 58-63, 2002.